Polarimetric BRDF in the Microfacet Model: Theory and Measurements

March 2000

Richard G. Priest
Naval Research Laboratory
Washington, DC 20375

Thomas A. Germer
National Institute of Standards and Technology
Gaithersburg, MD

ABSTRACT

A key to modeling polarimetric signatures of painted objects is the polarimetric bidirectional reflectance distribution function (BRDF). In particular, it is important to correctly capture the out-of-plane behavior of the BRDF. From the theoretical point of view, the BRDF is a complex object – a 4 x 4 matrix of functions, each depending on three angles. Brute force tabulation of such an object is unlikely to ever be a feasible modeling approach. For this reason, model forms of the BRDF, rooted in physics, are very valuable for extending measured data and for use in modeling codes. Only a limited number of such models have been mentioned in the literature. Perhaps the one most relevant to paints, such as CARC (Chemical Agent Resistive Coating) coatings, is the microfacet model. Unpolarized versions of this model have been used in various forms for years. This paper presents a full polarimetric version of this model and discusses its properties. Recently acquired polarimetric data is compared with the model. It is found that the model is successful in capturing qualitative aspects of this data.

1. Introduction

An important issue in polarimetric target signature modeling is the form of the polarimetric bidirectional reflectance distribution function (BRDF)[1,2]. The general form of the polarimetric BRDF, a 4 x 4 matrix function, is very complex with subtle constraints linking the sixteen elements. Since quantities such as the degree of polarization involve the difference of large numbers (to form a small number), details of the form of the BRDF are potentially quite important. This is especially true for out-of-plane scattering geometries. There is a clear advantage in working with a closed form expression which derives from a physical model, exhibits reciprocity symmetry, and integrates correctly to the directional reflectivity. Calculations using such a BRDF will be free of artifacts that could arise, for example, from using an interpolation of laboratory measurements not obeying the constraints among the sixteen elements. This paper presents the closed form result for the polarimetric BRDF derived from the microfacet model.

Report Documentation Page

Report Date	Report Type	Dates Covered (from... to)
00032000	N/A	-

Title and Subtitle Polarimetric BRDF in the Microfacet Model: Theory and Measurements	**Contract Number**
	Grant Number
	Program Element Number
Author(s) Priest, Richard G.; Germer, Thomas A.	**Project Number**
	Task Number
	Work Unit Number
Performing Organization Name(s) and Address(es) Naval Research Laboratory Washington, DC 20375	**Performing Organization Report Number**
Sponsoring/Monitoring Agency Name(s) and Address(es) Director, CECOM RDEC Night Vision and Electronic Sensors Directorate, Security Team 10221 Burbeck Road Ft. Belvoir, Va 22060-5806	**Sponsor/Monitor's Acronym(s)**
	Sponsor/Monitor's Report Number(s)
Distribution/Availability Statement Approved for public release, distribution unlimited	
Supplementary Notes	
Abstract	
Subject Terms	
Report Classification unclassified	**Classification of this page** unclassified
Classification of Abstract unclassified	**Limitation of Abstract** UNLIMITED
Number of Pages 13	

The microfacet model is rooted in geometric optics. Various forms of this model have been in the literature since the 1960s.[3-6] In its simplest form the model envisions a collection of randomly oriented microfacets as comprising the rough surface. Each microfacet acts as a specular reflector. A statistical distribution of facet orientations described by a distribution function is postulated. Only a reflection law for the microfacets, such as that provided by the Fresnel relations, is needed to complete a definition of the model. The literature contains several derivations of the scalar (unpolarized) BRDF arising from this model. These treatments use a variety of approaches and notations. Rather than review this derivation here, the scalar result is simply quoted.

An important relation links the unpolarized BRDF, f, to the directional hemispherical reflectivity (DHR),

$$DHR(\theta_i) = \int d^2\omega_r f(\theta_i, \theta_r, \phi_r - \phi_i)\cos(\theta_r). \tag{1}$$

The BRDF is a function of the incident polar angle θ_i, the scattered polar angle θ_r, and the difference between the incident and scattered azimuthal angles, $\phi_r - \phi_i$, where we assume the sample is rotationally symmetric. The solid angular integration is over the hemisphere above the surface. The integration differential, $d^2\omega_r$, is given by $\sin(\theta_r)\, d\theta_r\, d\phi_r$. Further, the scalar BRDF must be an even function of $\phi_r - \phi_i$. The cosine in the integrand appears because the BRDF is defined as being per unit projected area. Eq. (1) is a normalization condition on the BRDF. An ideal Lambertian reflecting surface has the property that the outgoing power per unit solid angle, per unit projected area, is independent of angle. This leads to the result that $f = 1/\pi$, that is, a constant, for the Lambertian case. Another important result concerns the radiance reflected from a horizontal surface exposed to an incoming sky radiance profile $R_{sky}(\theta_{sky})$. The definition of the BRDF leads to the result

$$R_{reflected}(\theta_r) = \int d^2\omega_{sky} f(\theta_{sky}, \theta_r, \phi_r - \phi_{sky}) R_{sky}(\theta_{sky})\cos(\theta_{sky}). \tag{2}$$

This result generalizes immediately to the case where the sky radiance depends on the azimuthal coordinate. It is the main result needed for modeling reflected signatures. Consideration of the process reciprocal to that leading to the expression for the DHR leads to a reciprocity condition on the BRDF. These can be written as

$$\int f(\theta_i, \theta_r, \phi_r - \phi_i)\cos(\theta_i) d^2\omega_i = RHO(\theta_r)$$

$$\int f(\theta_i, \theta_r, \phi_r - \phi_i)\cos(\theta_r) d^2\omega_r = RHO(\theta_i) \tag{3}$$

where $d^2\omega = \sin(\theta) d\theta d\phi$. The functional forms on the right-hand sides of Eqs. (3) are the same for both integrals and is the functional form of the DHR . A sufficient condition on f to insure this reciprocity condition is

$$f(\theta_i, \theta_r, \phi) = f(\theta_r, \theta_i, \phi). \tag{4}$$

As will be seen below, the microfacet model assumption leads to a form obeying this interchange symmetry.

The BRDF is closely related to another object, σ, which appears in some of the older literature[3]. This object is the differential scattering cross section per unit illuminated area. The definition of a differential scattering cross section implies that the power per unit solid angle going into the viewing direction is the product of the incident flux and the differential scattering cross section. It can be shown that the BRDF is related to σ by a simple relation,

$$f = \frac{\sigma}{\cos(\theta_r)\cos(\theta_i)}. \tag{5}$$

2. Definitions of angles

Some angular definitions were introduced in Section 1. This section collects all the notation used to refer to angles appearing in the sections below.

Three sets of spherical polar angles and associated unit vectors will prove to be useful. These are: 1) a unit vector $\mathbf{r}_i$, and associated polar and azimuthal angles θ_i and ϕ_i, pointing to the direction of the source radiation; 2) a unit vector $\mathbf{r}_r$, and associated angles θ_r and ϕ_r, pointing toward the position of a viewer; 3) a unit vector **n**, and associated angles θ and ϕ, pointing in the direction of the local surface normal of a microfacet. For each of these three, the symbol ω (with appropriate subscript in the case of the first two) will be used to refer to the polar, azimuth pair. The corresponding two-dimensional differential element is $d^2\omega = \sin(\theta)\, d\theta\, d\phi$. The overall surface normal will be denoted as **z** and this direction will serve as the polar axis for the spherical polar coordinates. A useful auxiliary angle is β, the angle of incidence onto or angle of reflection from a microfacet. In the microfacet model these are the same angle, and we have

$$\cos(\beta) = \mathbf{n}\cdot\mathbf{r}_i = \mathbf{n}\cdot\mathbf{r}_r. \tag{6}$$

Also following from the assumed mirror-like nature of a microfacet is the vector relation

$$\mathbf{r}_i + \mathbf{r}_r = 2\cos(\beta)\mathbf{n}\,. \tag{7}$$

Useful equations can be obtained from this vector relation by forming dot products with both sides. For example, taking the dot product of Eq. (7) with **z** leads to

$$\cos(\theta) = \frac{\cos(\theta_i)+\cos(\theta_r)}{2\cos(\beta)}\,. \tag{8}$$

3. Formal definition of the microfacet model

The microfacet model assumes that a collection of small microfacets comprises the rough surface. Each microfacet is a specular reflector obeying Snell's law of reflection (angle of incidence equal angle of reflection) with reflectivity given by a Fresnel reflectivity[7], $\rho(\beta)$, depending on the local angle of incidence, β. Each microfacet is characterized by a normal unit vector **n**, and the microfacets are assumed to be distributed symmetrically about **z** in orientation according to a distribution. A well-studied example is the Gaussian form,

$$p(\theta) = \frac{1}{2\pi\sigma^2\cos^3(\theta)}\exp\left(\frac{-\tan^2(\theta)}{2\sigma^2}\right)\,. \tag{9}$$

This is a normalized form, so that

$$\int d^2\omega\, p(\theta) = 1\,, \tag{10}$$

where the integral is over the upper hemisphere. The local surface slope is tan(θ). The slope variance is σ^2. This form can be shown to arise from the assumption of a Gaussian surface height distribution,[8] and has the advantage of enforcing $\theta < \pi/2$.

4. The scalar BRDF

Here the result for the scalar BRDF is quoted without derivation. The scalar BRDF is[3-6]

$$f = \frac{1}{2\pi}\frac{1}{4\sigma^2}\frac{1}{\cos^4(\theta)}\frac{\exp(-\frac{\tan^2(\theta)}{2\sigma^2})}{\cos(\theta_r)\cos(\theta_i)}\rho(\beta). \tag{11}$$

In working with Eq. (11), we can use:

$$\cos(\theta) = \frac{\cos(\theta_i)+\cos(\theta_r)}{2\cos(\beta)}$$

$$\cos(2\beta) = \cos(\theta_i)\cos(\theta_r)+\sin(\theta_i)\sin(\theta_r)\cos(\phi_i-\phi_r) \tag{12}$$

with the former being a restatement of Eq. (8) and the latter expression coming from the spherical addition theorem.

With these auxiliary formulas, it can be seen that the above expression for f has the interchange symmetry discussed in Section 1 and thus obeys the reciprocity condition. This expression agrees, apart from a factor of 4π, with the result for the differential scattering cross section derived in Ref. 3. The factor of 4π results from the way the differential scattering cross section is defined and normalized in Ref. 3.

5. Properties of the BRDF

In addition to the interchange symmetry, we note here another property of the microfacet BRDF. If $\rho(\beta) = 1$, then

$$\int d^2\omega_r \cos(\theta_r) f(\theta_i, \theta_r, \phi_r - \phi_i) = DHR(\theta_i) = 1 \tag{13}$$

for any value of θ_i. The integration over ω_r is rather involved because of the non-trivial out-of-plane behavior of f. Rather than attempt this integration analytically, the commercial program MATHCAD* was used to carry out this integration for a representative set of values of θ_i. The result was as expected, the integral always evaluates to unity. In getting this result it was necessary to allow θ_r to range over [0 ,

* Certain commercial equipment, instruments, or materials are identified in this paper in order to specify the experimental procedure adequately. Such identification is not intended to imply recommendation or endorsement by the National Institute of Standards and Technology or the Naval Research Laboratory, nor is it intended to imply that the materials or equipment identified are necessarily the best available for the purpose.

π] rather than be confined to the upper hemisphere (the surround) [0, $\pi/2$]. The physical meaning of this finding is that the model, as outlined above, allows radiation to be scattered below the surface. In fact, this is not possible; such radiation would be multiply scattered and a portion would emerge above the surface. From the practical point of view, this is not a serious problem. For reasonable choices of σ, the contribution to the integral from the range [$\pi/2$, π] is small. In fact, the light scattered below the surface by the model can be thought of as contributing an unpolarized Lambertian term to the BRDF. This idea could be developed into a model for a depolarizing contribution to the BRDF.

6. Polarization

The discussion to this point has been presented in the context of unpolarized electromagnetic radiation. However, it can be readily generalized to the case of polarized radiation. The reason that the generalization is straightforward is that the microfacet model is deterministic in nature. Once the incident and scattering angles are specified, the orientation of the reflecting microfacet is fully determined. A consequence is that the model does not depolarize radiation[9]. If the incident radiation has a degree of polarization, DOP = 1, the scattered radiation, at any scattering angle, will also have DOP = 1. This allows a Jones matrix approach to be followed below. The idea for using the Jones matrix approach was mentioned in Ref. 3, but the results there are not presented in the useful form of Eq. (14) below, nor is the route to the derivation clear.

The generalization of the material in Sec. 1 that we desire is to describe radiances by four-component Stokes vectors and to find a 4 x 4 matrix generalization of the function f. This suggests, correctly, that f should have the properties of a Mueller matrix.

For the purposes of this section θ_i, θ_r, and $\phi_r - \phi_i$ are considered to be fixed. This also fixes the orientation of the reflecting microfacet and the angles θ and β through Eqs. (12). The derivation is similar to that of the scalar facet model, except that the vector nature of the reflection coefficient ρ must be taken into account.

The Jones matrix involves the electric field vectors. It is necessary to introduce a series of four 2-dimensional (x,y) coordinate systems to track the electric field though the scattering process. The axes of these coordinate systems are the familiar s and p of Fresnel reflection theory. The designation s means perpendicular to a reference plane, and the designation p means parallel to the reference plane, both are perpendicular to a propagation direction. For the first coordinate system, the reference plane is defined by the incident direction and the surface normal **z.** For the second coordinate system the reference plane is defined by the microfacet normal **n** and the incident direction. The second coordinate system is rotated away from the first (about the incident direction) by an angle η_i. It will be seen below that η_i is a function of θ_i, θ_r, and $\phi_r - \phi_i$. For the third coordinate system, the reference plane is defined by the microfacet normal **n** and the reflected direction. This reference plane is the same as for the second coordinate system but the propagation direction (needed to specify p) is now the reflected direction. For the fourth coordinate system, the reference plane is defined by the reflected direction and the surface normal **z**. The fourth coordinate system is rotated away from the third (about the reflected direction) by an angle $-\eta_r$. In general, the angle η_r is not equal to η_i, but is also determined uniquely by θ_i, θ_r, and $\phi_r - \phi_i$.

The Fresnel amplitudes for ss (a_{ss}) and pp (a_{pp}) reflection relate the reflected electric field, as described in the third coordinate system, to the incident electric field, as described in the second coordinate system. Schematically this can be represented as $\mathbf{E}_r = a\ \mathbf{E}_i$ where a is a complex diagonal 2 x 2 matrix. What is needed is the Jones matrix, a 2 x 2 matrix relating the reflected electric field, as described in the fourth coordinate system, to the incident electric field, as described in the first coordinate system. With the aid of the angles η_i and η_r, and rotation matrices, this can be given as:

$$\begin{pmatrix} E_s^r \\ E_p^r \end{pmatrix} = \begin{pmatrix} \cos(\eta_r) & \sin(\eta_r) \\ -\sin(\eta_r) & \cos(\eta_r) \end{pmatrix} \begin{pmatrix} a_{ss} & 0 \\ 0 & a_{pp} \end{pmatrix} \begin{pmatrix} \cos(\eta_i) & -\sin(\eta_i) \\ \sin(\eta_i) & \cos(\eta_i) \end{pmatrix} \begin{pmatrix} E_s^i \\ E_p^i \end{pmatrix}$$
$$\begin{pmatrix} E_s^r \\ E_p^r \end{pmatrix} = \begin{pmatrix} T_{ss} & T_{ps} \\ T_{sp} & T_{pp} \end{pmatrix} \begin{pmatrix} E_s^i \\ E_p^i \end{pmatrix} \tag{14}$$

The second relationship is the working definition of the Jones matrix, T. Here a_{ss} and a_{pp} are Fresnel amplitudes, not reflectivities. In general they are complex functions of β and, through β, functions of θ_i, θ_t, and $\phi_t - \phi_i$. Explicit forms for the elements of the Jones matrix in terms of a_{ss}, a_{pp}, η_i and η_r can be easily worked by carrying out the matrix multiplications above.

To complete the analysis it is necessary to give an expression relating the Mueller matrix elements to those of the Jones matrix, and to provide explicit expressions for η_i and η_r. Reference 9 gives a formal relation between the Jones matrix, T, and the Mueller matrix, M. Perhaps more directly useful are the explicit formulas found in Bohren and Huffman[10]. Allowing for differences in notation these are:

$$\begin{aligned}
M_{00} &= \tfrac{1}{2}(|T_{ss}|^2 + |T_{sp}|^2 + |T_{ps}|^2 + |T_{pp}|^2) \\
M_{01} &= \tfrac{1}{2}(|T_{ss}|^2 + |T_{sp}|^2 - |T_{ps}|^2 - |T_{pp}|^2) \\
M_{02} &= \tfrac{1}{2}(T_{ss}T_{ps}^* + cc \quad + T_{sp}T_{pp}^* + cc) \\
M_{03} &= \tfrac{1}{2}[i(T_{ps}T_{ss}^* - cc) + i(T_{pp}T_{sp}^* - cc)] \\
M_{10} &= \tfrac{1}{2}(|T_{ss}|^2 - |T_{sp}|^2 + |T_{ps}|^2 - |T_{pp}|^2) \\
M_{11} &= \tfrac{1}{2}(|T_{ss}|^2 - |T_{sp}|^2 - |T_{ps}|^2 + |T_{pp}|^2) \\
M_{12} &= \tfrac{1}{2}[(T_{ss}T_{ps}^* + cc) \quad - (T_{sp}T_{pp}^* + cc)] \\
M_{13} &= \tfrac{1}{2}[i(T_{ps}T_{ss}^* - cc) - i(T_{pp}T_{sp}^* - cc)] \\
M_{20} &= \tfrac{1}{2}(T_{ss}T_{sp}^* + cc \quad + T_{ps}T_{pp}^* + cc) \\
M_{21} &= \tfrac{1}{2}[(T_{ss}T_{sp}^* + cc) \quad - (T_{ps}T_{pp}^* + cc)] \\
M_{22} &= \tfrac{1}{2}(T_{ss}T_{pp}^* + cc \quad + T_{ps}T_{sp}^* + cc) \\
M_{23} &= \tfrac{1}{2}[i(T_{ps}T_{sp}^* - cc) - i(T_{ss}T_{pp}^* - cc)] \\
M_{30} &= \tfrac{1}{2}[i(T_{ss}T_{sp}^* - cc) + i(T_{ps}T_{pp}^* - cc)] \\
M_{31} &= \tfrac{1}{2}[i(T_{ss}T_{sp}^* - cc) - i(T_{ps}T_{pp}^* - cc)] \\
M_{32} &= \tfrac{1}{2}[i(T_{ss}T_{pp}^* - cc) + i(T_{ps}T_{sp}^* - cc)] \\
M_{33} &= \tfrac{1}{2}[(T_{ss}T_{pp}^* + cc) \quad - (T_{ps}T_{sp}^* + cc)]
\end{aligned} \tag{15}$$

Here the asterisk denotes the operation of taking the complex conjugate, cc stands for complex conjugate of the immediately preceding expression, and i is the imaginary unit.

The expression for the polarimetric BRDF is therefore

$$f_{j,k}(\theta_i,\theta_r,\phi_r-\phi_i)=\frac{1}{2\pi}\frac{1}{4\sigma^2}\frac{1}{\cos^4(\theta)}\frac{\exp(-\frac{\tan^2(\theta)}{2\sigma^2})}{\cos(\theta_r)\cos(\theta_i)}M_{j,k}(\theta_i,\theta_r,\phi_r-\phi_i) \tag{16}$$

where j and k each range from 0 to 3. In an expression such as Eq. (2) , R_{sky} and $R_{reflected}$ are replaced by Stokes vectors, and the scalar BRDF is replaced by the matrix form above.

Eq. (15) simplifies in some cases. For the case of in-plane scattering ($\phi_r-\phi_i=0$), $\eta_i = \eta_r = 0$, and the off diagonal elements of the Jones matrix are zero. This leaves only M_{00}, M_{01}, M_{10}, M_{11}, M_{22}, M_{23}, M_{32}, and M_{33} non-zero, with $M_{01} = M_{10}$, $M_{00} = M_{11}$, $M_{22} = M_{33}$ and $M_{23} = -M_{32}$. This is the pattern often seen in literature discussions of the Mueller matrix. The fact that $M_{00} = M_{11}$ for this case is indicative of the fact that there is no depolarization in this model. A simpler case occurs when all elements of the Jones matrix are real, which is the situation in Fresnel theory when the index of refraction is real. In this case $M_{03} = M_{30} = M_{13} = M_{31} = M_{23} = M_{32} = 0$, and no circular polarization can be generated unless the incident radiation has a circular component.

The remaining task is to give expressions for the angles η_i and η_r in terms of θ_i, θ_r, and $\phi_r-\phi_i$. For this purpose it is useful to introduce four unit vectors[11]. These are $\mathbf{S}_i$, $\mathbf{\Sigma}_i$, $\mathbf{S}_r$, and $\mathbf{\Sigma}_r$. As above, the subscript i refers to the incident ray and the subscript r to the reflected ray. The $\mathbf{S}_i$, unit vector is perpendicular to the incident direction and to the **z** direction. It is parallel to the electric field for radiation polarized perpendicular to the reference plane in the first of the four coordinate systems defined above. The $\mathbf{\Sigma}_i$ unit vector is perpendicular to the incident direction and to the **n** direction. It is parallel to the electric field for radiation polarized perpendicular to the reference plane in the second of the four coordinate systems. The $\mathbf{\Sigma}_r$ unit vector is perpendicular to the reflected direction and to the **n** direction. It is parallel to the electric field for radiation polarized perpendicular to the reference plane in the third coordinate system. Finally, the $\mathbf{S}_r$ unit vector is perpendicular to the reflected direction and to the **z** direction. It is parallel to the electric field for radiation polarized perpendicular to the reference plane in the fourth coordinate system. These four unit vectors can be related to the unit vectors introduced earlier by the cross product relations:

$$\begin{aligned}
\mathbf{S}_i &= (\mathbf{r}_i\times\mathbf{z})/|\mathbf{r}_i\times\mathbf{z}| = (\mathbf{r}_i\times\mathbf{z})/\sin(\theta_i)\\
\mathbf{\Sigma}_i &= (\mathbf{r}_i\times\mathbf{n})/|\mathbf{r}_i\times\mathbf{n}| = (\mathbf{r}_i\times\mathbf{n})/\sin(\beta)\\
\mathbf{S}_r &= -(\mathbf{r}_r\times\mathbf{z})/|\mathbf{r}_r\times\mathbf{z}| = -(\mathbf{r}_r\times\mathbf{z})/\sin(\theta_r)\\
\mathbf{\Sigma}_r &= -(\mathbf{r}_r\times\mathbf{n})/|\mathbf{r}_r\times\mathbf{n}| = -(\mathbf{r}_r\times\mathbf{n})/\sin(\beta)\\
\mathbf{n} &= (\mathbf{r}_i+\mathbf{r}_r)/(2\cos(\beta))
\end{aligned} \tag{17}$$

The expression for **n** is repeated from Eq. (7) above. From these definitions it can be seen that

$$\begin{aligned}
\cos(\eta_i) &= \mathbf{S}_i\cdot\mathbf{\Sigma}_i = (\mathbf{r}_i\times\mathbf{z})\cdot(\mathbf{r}_i\times\mathbf{n})/(\sin(\theta_i)\sin(\beta)) = \frac{[\mathbf{n}\cdot\mathbf{z}-(\mathbf{r}_i\cdot\mathbf{z})(\mathbf{r}_i\cdot\mathbf{n})]}{\sin(\theta_i)\sin(\beta)}\\
\cos(\eta_r) &= \mathbf{S}_r\cdot\mathbf{\Sigma}_r = (\mathbf{r}_r\times\mathbf{z})\cdot(\mathbf{r}_r\times\mathbf{n})/(\sin(\theta_r)\sin(\beta)) = \frac{[\mathbf{n}\cdot\mathbf{z}-(\mathbf{r}_r\cdot\mathbf{z})(\mathbf{r}_r\cdot\mathbf{n})]}{\sin(\theta_r)\sin(\beta)}
\end{aligned} \tag{18}$$

A standard vector identity was used to eliminate the cross products. The expression for **n** given in Eq. (7) can be substituted into these expression to reduce this expression to trigonometric functions of θ_i, θ_r, and β. The results can be written as:

$$\cos(\eta_i) = [(\cos(\theta_i) + \cos(\theta_r))/(2\cos(\beta)) - \cos(\theta_i)\cos(\beta)]/(\sin(\theta_i)\sin(\beta))$$
$$\cos(\eta_r) = [(\cos(\theta_i) + \cos(\theta_r))/(2\cos(\beta)) - \cos(\theta_r)\cos(\beta)]/(\sin(\theta_r)\sin(\beta)) \quad (19)$$
$$\cos(2\beta) = \cos(\theta_i)\cos(\theta_r) + \sin(\theta_i)\sin(\theta_r)\cos(\phi_r - \phi_i)$$

The equation for $\cos(2\beta)$ follows from the spherical addition theorem. These three equations constitute the expression for the angles η_i and η_r in terms of θ_i, θ_r, and $\phi_r - \phi_i$. It can be easily checked that $\eta_i = \eta_r = 0$ when and $\phi_r = \phi_i$.

7. Visualization of the BRDF

The analytic formulas above are too complex to allow the character of the BRDF to be directly apprehended. Contour plots in the θ_r, ϕ_r plane (for fixed incident direction) are a useful way to visualize the structure of the BRDF. This section presents examples of this type of plot. The values of the parameters have been chosen not to match data but to allow certain key features to be easily seen. As a further aid to visualization, the quantity plotted is the product of the BRDF component and $\cos(\theta_r)$. Without multiplication by this factor of cosine, the in-plane BRDF diverges as θ_r approaches 90 degrees. This divergence is real in the sense that it is seen in measured data where the effective value of σ is less than about 1.5. The divergence is confined to near in-plane angles and does not present problems in practical use of the BRDF because of the cosine factors in integration formulas such as Eq. (1) and (2).

The parameter values chosen for Figs. 1–4 are $\sigma = 0.15$, and index of refraction $n = 1.57$, with an incidence angle of 60 degrees. Since the value of n is real, the symmetries discussed in the previous section apply and Brewster angle effects are significant. Contour plots for the 00, 02, 22 and 33 matrix elements are shown in Figs. 1 through 4, respectively. In-plane scattering corresponds to $\phi = 0$ degrees in these plots. It can be noted the 00 and 11 components peak near the specular scattering direction as expected. However, their behavior out-of-plane is significantly different. The general behavior of the 01 component (not shown) is similar to that of the 00 component. The 22 component shows dramatic effects of passing through the Brewster angle. The track of the Brewster angle position can be seen in the θ_r, ϕ_r plane. The 02 component is zero for in-plane scattering as expected from symmetry. The contour plot shows a peak approximately 10 degrees removed from the in-plane condition. The 12 component (not shown) exhibits similar behavior. The complex behavior of these off-diagonal components suggests the attempts to fit to simple functional forms will encounter difficulties.

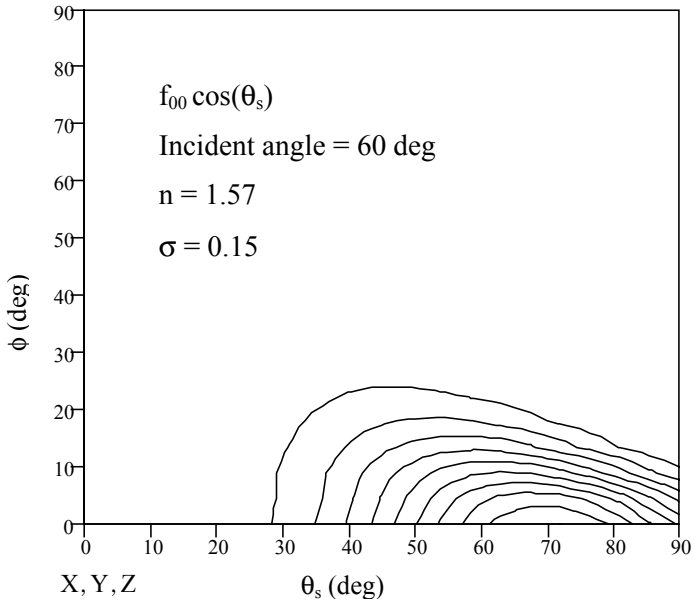

Figure 1

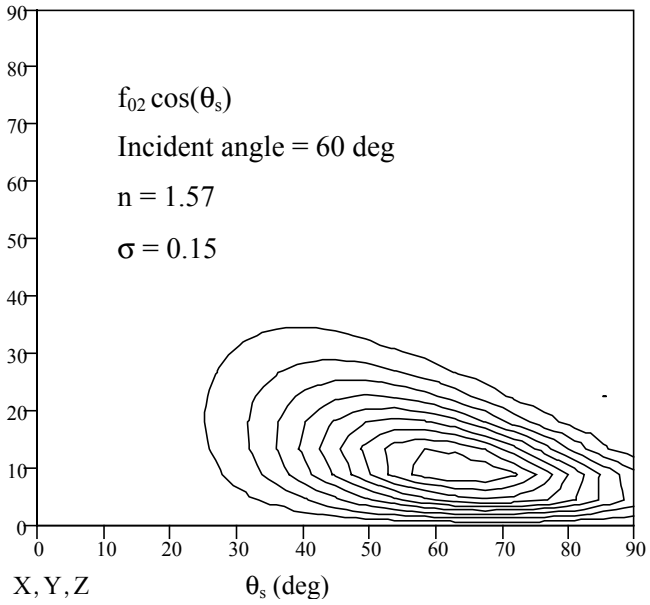

Figure 2

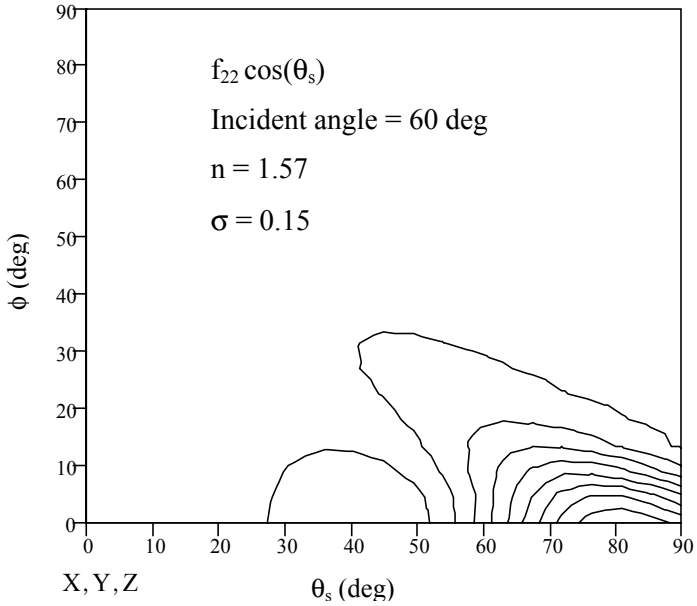

Figure 3

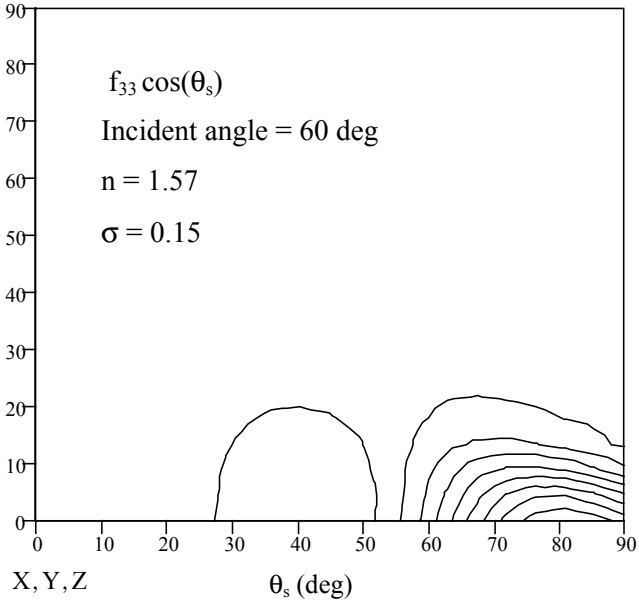

Figure 4

8. Comparison with measurements

The ideal data set for comparison purposes would feature full polarimetric measurements, both in-plane and out-of-plane, at several wavelengths. Such a full data set does not appear to exist. We have obtained data sets measured on metal coupons painted with CARC Green 383 paint from Surface Optics Corporation (SOC)[12] and from the National Institute of Standards and Technology (NIST). The SOC data set is limited to in-plane data, but is polarimetric and contains measurements at three representative wavelengths (0.50 μm, 4.60 μm and 9.925 μm). The NIST data, while confined to the visible (0.633 μm), features (partial) polarimetric measurements for both in-plane and out-of-plane geometries. This section presents a preliminary investigation of the fit between the microfacet model and the measured data.

The model described above has just three parameters, the slope distribution width parameter σ, and the real and imaginary parts of the index of refraction n. It is a rather strenuous exercise to fit a tensor function over three angles with just three parameters. As will be seen below, the model predicts major trends correctly but is not a close numerical fit. For this preliminary investigation, the parameters are used freely as fit parameters with only general reasonability used as a constraint.

In the case of the visible (0.633 μm) measurements, the parameter space reduces to two because it is not expected that the imaginary part of the index of refraction would play a major role. A small, but not negligible, amount of depolarized scattering is evident on examining the NIST data set. As discussed above, this contribution to the BRDF is not modeled by the microfacet model. In the NIST measurements[†], the sample was illuminated with *s*- or *p*-polarized radiation, and the BRDF was recorded. A first order empirical allowance for the depolarized scattering can be made by introducing a diffuse contribution additive to the model BRDF. In the figures below this is taken as a constant additive contribution of 0.025 sr^{-1} to the BRDF for the case of *p*-polarized incident radiation, and a contribution of 0.04 sr^{-1} for s-polarized incident radiation.

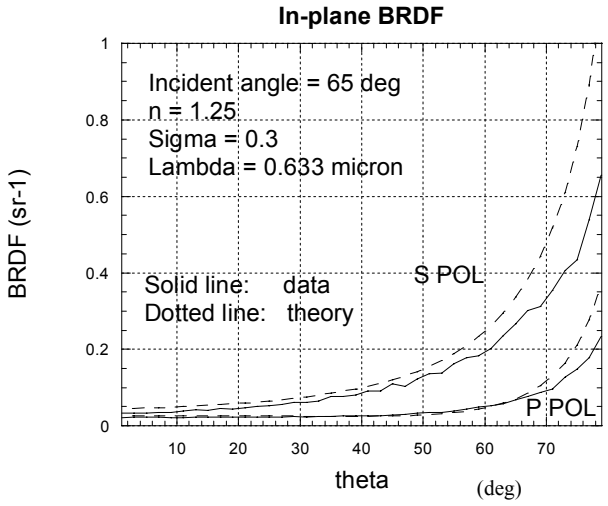

Figure 5

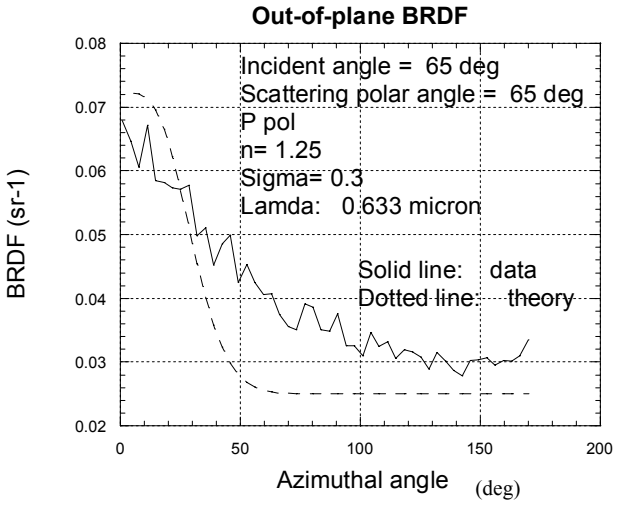

Figure 6

[†]The uncertainties in the data are dominated by statistical sources, and can be estimated by the point-to-point spread in the data. Other sources of uncertainty are expected to be below 3 % of any given value.

Figure 5 shows the in-plane BRDF for an incident angle of 65 degrees, shown as a function of polar scattering angle. The model parameters are as shown in the text box in the figure. The theoretical curves are $(f_{00}+f_{01})$ + 0.04 for the case of *s*-polarization and $(f_{00}-f_{01})$ + 0.025 for the case of *p*-polarization. As can be seen from the curves, the qualitative features of the data are captured by the model. Light which is s-polarized is always more strongly scattered than light which is *p*-polarized, and there is no discernable peak at the specular scattering angle of 65 degrees. The BRDF diverges as the polar scattering angle approaches 90 degrees. However, there is no combination of the two parameters (n and σ) which match the BRDF over the whole angular range. For the parameter choice shown, the divergence is weaker in the data than predicted by the model. Further the value n = 1.25 is lower than might have been expected on physical grounds.

Figure 6 shows the out-of-plane BRDF for *p*-polarized radiation, shown as a function of azimuthal angle for fixed polar angles (both incident and scattering) of 65 degrees. As with the case of the in-plane data, the qualitative features are captured but quantitative agreement is not obtained. The wide width seen in the data indicates that the functional form of the actual slope distribution falls off more gently than the exponential form used in the model.

The NIST data also allows the degree of polarization (DOP) to be studied. For the out-of-plane data of Fig. 6, the DOP decreases as the azimuthal angle increases from about 0.7 to about 0.4. This is roughly consistent with the model predictions assuming that the 0.025 additive contribution is approximately correct.

A different test of the polarization performance of the microfacet model can be made by an examination of the orientation of the principal direction of linear polarization, $\eta^{(p)}$, as the azimuthal scattering angle is varied. For the data of Fig.7 the incident radiation is *p*-polarized and both the incident and scattering polar angles are set at 45 degrees. The scattering azimuth is varied, and the orientation of the principal direction is plotted. A value of 90 degrees for this angle means that the scattered linearly polarized light is *p*-polarized, while a value of 0 degrees corresponds to *s*-polarization. As can be seen from the Fig. 7, the scattered light is *p*-polarized for in-plane scattering (as expected from symmetry) and tends to be *s*-polarized as the scattering azimuth increases away from the in-plane configuration. A very good fit of the microfacet model to the data was possible with a choice of n = 1.5.

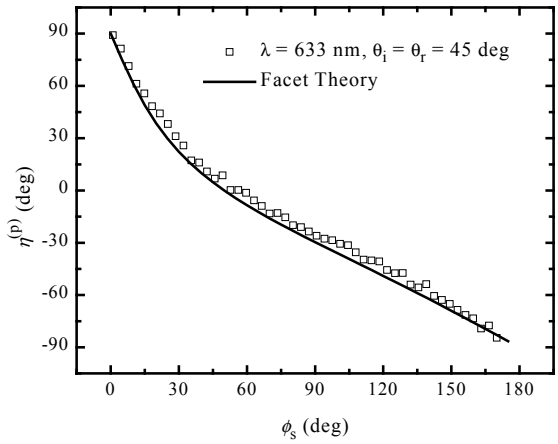

Figure 7

Figures 8 and 9 present an in-plane BRDF measured at SOC using 9.925 μm radiation.[12] In Fig. 8, the f_{00} component, for incident angle equal to 60 degrees, is plotted as a function of polar scattering angle. The model parameters are shown in the figure. The f_{10} component is shown in Fig. 9. For the 9.925 μm radiation case it is necessary to include an imaginary part of the index of refraction to get qualitative

agreement between measurements and the model. However, the depolarized diffuse contribution is relatively smaller and can be neglected for purposes of this preliminary analysis.

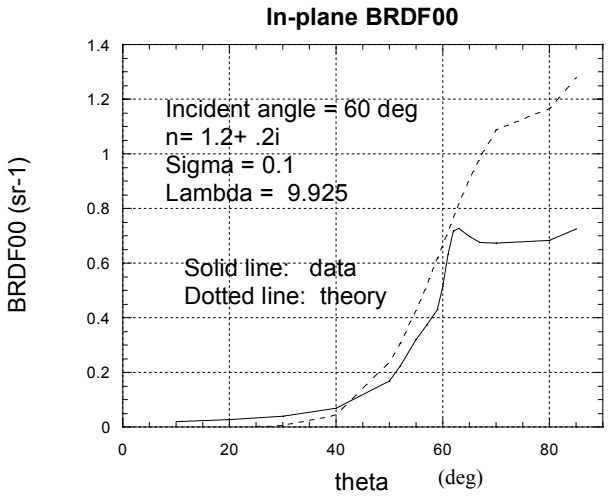

Figure 8

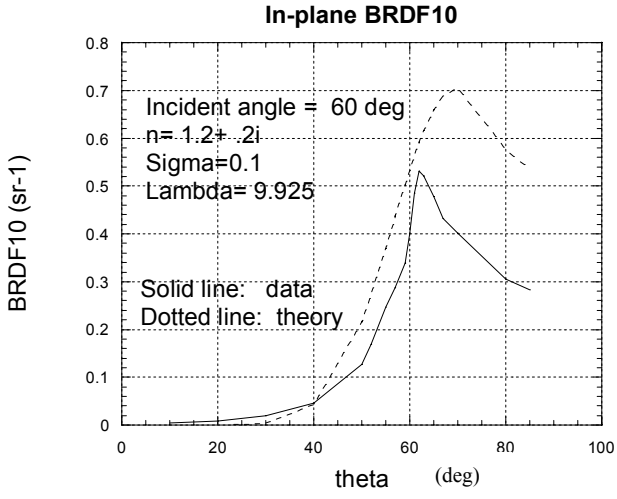

Figure 9

As can be seen in the figures, qualitative features of the data are captured by the model. There is a peak near the specular scattering angle (60 degrees) which is shifted to larger angle by the (weak) divergence as 90 degrees is approached. The numerical values are in the correct range until past the specular angle. The modulus of the complex index of refraction chosen to obtain the fit is lower than would be expected on physical grounds.

The fit value of the model width parameter, σ, is only 0.1 for the 9.925 μm case as compared with 0.3 for the visible case. In the model calculations, this is why the 9.925 μm BRDF shows a peak at the specular scattering angle while the visible BRDF does not. It is reasonable to ascribe the difference in behavior at the two wavelength regions to diffraction effects not directly modeled in the microfacet model. A non-rigorous argument can be advanced to motivate the use of a smaller value of σ for the 9.925 μm case than for the 0.633 μm case. The value of σ^2 is the value of the surface slope variance. The variance can be viewed as the integral, over wavenumber, of the power spectral density of surface slope. To perform the integral, an upper wavenumber cut-off must be selected. The higher the cut off, the larger the resulting variance. It is reasonable to argue that diffraction effects should set the cut –off at roughly $2\pi/\lambda$ where λ is the wavelength of the light being scattered. This argument suggests that the cut off for 0.633 μm light is some 20 times higher than for the 9.925 μm light

9. Summary

Closed form expressions for the full polarimetric form of the BRDF has been derived for the microfacet model. Numerical study of this result reveals complex structure for some of the individual components of the BRDF, especially the off-diagonal elements. Comparisons with measured data indicate that the three parameter model captures important qualitative features of the data but falls well short of numerical agreement.

10. References

1) J.C. Stover, *Optical Scattering*, McGraw Hill, 1990, p. 16.

2) F. Nicodemus, Appl. Opt. **4**, p. 767, 1965.

3) D.E. Barrick, IEEE Trans. Antennas and Prop. **AP-16**, p. 449, 1968.

4) T.S. Trowbridge and K.P. Reitz, J. Opt. Soc. Amer. **65**, p. 531, 1975.

5) K.E. Torrance and E.M. Sparrow, J. Opt. Soc. Amer. **57**, p. 1105, 1967.

6) J. Beard and J.R. Maxwell, Technical Report Number AFAL-TR-73-303 (1973).

7) See for example M. Born and E. Wolf, *Principles of Optics*, Pergamon Press 1986.

8) R.G. Priest and I.B. Schwartz, NRL Memorandum Report 6092, 1988.

9) K. Kim, L. Mandel, E. Wolf, J. Opt. Soc. Amer. A, **4**, p. 433, 1987.

10) C.F. Bohren and D.R. Huffman, *Absorption and Scattering of Light by Small Particles*, Wiley-Interscience, 1983, p. 65.

11) This approach is motivated by T.A. Germer and C.C. Asmail, J. Opt. Soc. Amer. A , **16**, p. 1326, 1999.

12) SOC Technical Report SOC-R6001-071-001-0999, 1999.